NJC

Accepted Manuscript

This is an *Accepted Manuscript*, which has been through the Royal Society of Chemistry peer review process and has been accepted for publication.

Accepted Manuscripts are published online shortly after acceptance, before technical editing, formatting and proof reading. Using this free service, authors can make their results available to the community, in citable form, before we publish the edited article. We will replace this *Accepted Manuscript* with the edited and formatted *Advance Article* as soon as it is available.

You can find more information about *Accepted Manuscripts* in the Information for Authors.

Please note that technical editing may introduce minor changes to the text and/or graphics, which may alter content. The journal's standard Terms & Conditions and the Ethical guidelines still apply. In no event shall the Royal Society of Chemistry be held responsible for any errors or omissions in this *Accepted Manuscript* or any consequences arising from the use of any information it contains.

ROYAL SOCIETY OF CHEMISTRY

www.rsc.org/njc

Journal Name

RSCPublishing

ARTICLE

Well-dispersed ultrafine Mn_3O_4 nanocrystal on reduced graphene oxide with high electrochemical Li-storage performance

Cite this: DOI: 10.1039/x0xx00000x

Received 00th January 2014,
Accepted 00th January 2014

DOI: 10.1039/x0xx00000x

www.rsc.org/

Hui Huang, Liyuan Zhang, Yang Xia, Yongping Gan, Xinyong Tao, Chu Liang, Wenkui Zhang*

Graphene-based hybrid nanostructures could offer many opportunities for improved lithium storage performance. Herein, we report a novel synthesis of Mn_3O_4/reduced graphene oxide (Mn_3O_4/r-GO) composite based on microexplosion mechanism and reduction treatment. It is found that the well-dispersed ultrafine Mn_3O_4 particles with a size of about 20 nm are closely anchored on the surface of r-GO sheets. Compared to pure Mn_3O_4, the Mn_3O_4/r-GO composite delivers higher lithium storage capacity and superior rate capability as promising anode materials for Li-ion batteries. The enhanced electrochemical performance of the Mn_3O_4/r-GO composite can be attributed to the buffering confining and conducting effects of the r-GO sheets, as well as the small and uniform particle size of Mn_3O_4.

1. Introduction

Lithium ion batteries (LIBs) have attracted considerable interests as one of the most promising energy storage devices for high-power electric vehicles and portable electronic devices because of their attractive high energy density, cycling stability, and excellent rate capability.[1-3] On the basis of unique conversion reaction mechanism and high theoretical capacities, metal oxides (CoO_x,[4-6] FeO_x,[7-10] and MnO_x[11-15]) have received increasing attention as promising alternative anode materials to graphite. Compared with the other oxides, Mn_3O_4 exhibits high theoretical capacity (937 mAh g^{-1}), low conversion potential, natural abundance and environmental benignity, which are desirable for the practical application in LIBs.[16-19] However, the commercial use of pure Mn_3O_4 is still hampered by its low rate capability arising from the poor electrical conductivity (~10^{-7} to 10^{-8} S cm^{-1}), and rapid capacity fading because of severe particle agglomeration and drastic volume changes over extended cycling.

Up to date, enormous efforts have been made to circumvent these drawbacks. One effective strategy is to synthesize nanostructured Mn_3O_4 (nanofibers, nanorods) to shorten the diffusion length for electrons and lithium ions. Another efficient strategy is constructing nanocomposites with carbon materials like amorphous carbon shell,[20, 21] carbon nanotubes,[22] carbon nanofiber[23] and graphene sheets,[17, 18, 24-28] which act as both a volume buffer and a conductive network to absorb the internal stress and to increase ion and electron transport in the electrode. Compared to other carbon materials, graphene is a two-dimensional one-atom-thick conductor with high surface area, chemical stability, mechanical strength and flexibility, making it a potential carbon matrix for electrochemical energy storage applications.[29, 30] In addition, graphene contributes to the overall capacity. Li *et al.*[19] synthesized a nanocomposite of Mn_3O_4 wrapped in graphene sheets by microwave-assisted hydrothermal method, presenting high reversible capacity (more than 900 mAh g^{-1} at 40 mA g^{-1}). Cui *et al.*[18] reported two-step solution-phase reactions to synthesize Mn_3O_4/graphene hybrid, showing a high specific capacity up to ~900 mAh g^{-1} with good rate capability and cycling stability. Yi *et al.*[17] reported a one-step method for fabricating Mn_3O_4/graphene composite for use as anode material in LIBs. Different from these methods as mentioned, herein, we have developed a novel microexplosion method to synthesize the nanocomposite of Mn_3O_4 supported by r-GO sheets. Through this approach, the ultrafine Mn_3O_4 nanoparticles with a size of 20 nm are uniformly anchored on the r-GO sheets. The r-GO graphene sheets in the composite can not only efficiently buffer the volume change of Mn_3O_4 nanoparticles during charging and discharging processes, but also preserve the high electrical conductivity of the whole electrode. As a consequence, the Mn_3O_4/r-GO composite possesses high reversible capacity, good cycle life, and high rate capability as anode material for LIBs.

College of Materials Science and Engineering, Zhejiang University of Technology, Hangzhou 310014, China. Tel: 86-571-88320394, Email: msechem@zjut.edu.cn.

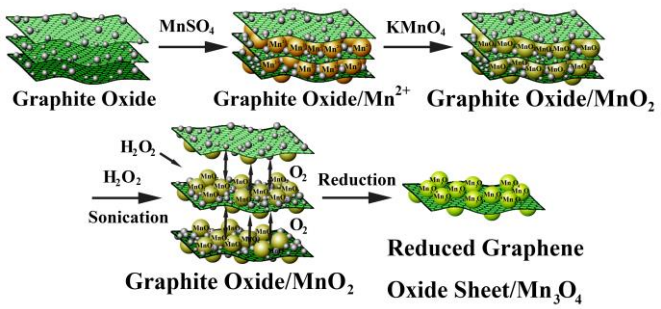

Figure 1 Schematic illustration of the synthesis steps of Mn_3O_4/r-GO composites based on a microexplosion mechanism.

2. Experimental Section

2.1 Synthesis of Mn_3O_4/r-GO composite

In a typical synthesis of the Mn_3O_4/r-GO composites, 0.16 g of GO, prepared by a improved Hummers method,[31, 32] was dispersed in deionization water with sonication for 1 h. Then, 3.75 g of $MnSO_4$ was added in the GO dispersion under stirring for 4 hours, and 2.79 g of $KMnO_4$ was added in the above solution with the reaction for 4 hours to form the MnO_2/r-GO composite. Subsequently, H_2O_2 is added dropwise under ultrasonic conditions and instantly releases a large amount of oxygen, which leads to the exfoliation of MnO_2/r-GO into nanosheets. Finally, 10 mL of hydrazine hydrate was added dropwise into the above solution in oil bath at 100°C with stirring for 24 hours. The resultant product was collected by centrifugation, and rinsed with deionized water and dried at 80°C overnight in a vacuum oven. For comparison, the bare Mn_3O_4 nanoparticles without adding GO and the Mn_3O_4/r-GO composite without adding H_2O_2 (without microexplosion reaction) were prepared by similar experimental procedures.

2.2 Materials characterization

The as-prepared samples were characterized by powder X-ray diffractometry (XRD, X' Pert Pro diffractometer with a Cu Kα radiation, λ=0.15418 nm), scanning electron microscopy (SEM, Hitachi S-4700) and transmission electron microscopy (TEM, FEI, Tecnai G2 F30), equipped with an energy dispersive spectroscopy (EDS) detector. Nitrogen adsorption-desorption isotherms were determined by Brunanuer-Emmett-Teller (BET) test using an ASAP 2020 (Micromeritics Instruments) surface area and pore analyzers.

2.3Electrochemical Measurements

Electrochemical measurements were performed by using CR2025 type coin cells, assembled in an Ar-filled glove box. The as-prepared Mn_3O_4/r-GO sample was mixed with acetylene black and polyvinylidenefluoride (PVDF) binder at a weight ratio of 75:15:10 in N-methyl-2-pyrrolidene (NMP) solution. The slurry was pasted on a Cu foil and dried in a vacuum oven at 120 °C for 12 h to serve as the working electrode. The weight of the active material in the electrode sheet was about 5 mg in a square centimeter of aluminum foil. A pure lithium foil was used as both counter electrode and reference electrode. A solution of 1M $LiPF_6$ in ethylene carbonate (EC)/dimethyl carbonate (DME) (1:1 by volume) was used as the electrolyte, and a polypropylene microporous film (Cellgard 2300) as the separator. The galvanostatical charge-discharge experiments were tested at different current densities in a voltage range of 0.01-3.0 V on a battery test system (Shenzhen Neware Battery, China). Cyclic voltammetry (CV) measurements were carried out on a CHI650B electrochemical workstation (Shanghai Chenhua, China). The CVs were obtained over the potential range of 0.01-3.0 V at a scanning rate of 0.1 mV s^{-1}.

3. Results and discussion

The Mn_3O_4/r-GO composites were prepared with graphite oxide as starting material. The chemical processes is shown in Figure 1. Mn^{2+} could be infiltrated sufficiently into graphite oxide (GO) sheets to form GO/Mn^{2+} composite, which is owing to the attraction of negatively charged oxygen-containing functional groups. After Mn^{2+} reacting with MnO_4^- and H_2O, the intercalation compound of MnO_2 could be formed within the layers of GO. When H_2O_2 was added under ultrasonic conditions, a microexplosion reaction occurred in the interlayer space of GO/MnO_2, resulting in the edges of GO/MnO_2 layers being exfoliated. The final Mn_3O_4/r-GO composite was obtained by hydrazine hydrate reduction.

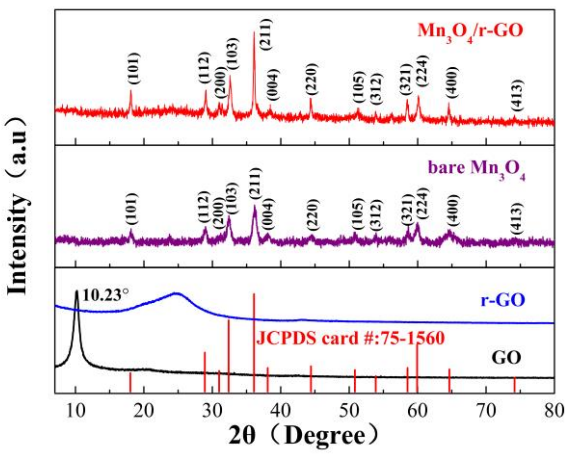

Figure 2 XRD patterns of Mn_3O_4/r-GO, bare Mn_3O_4, r-GO and GO

Figure 2 shows the XRD patterns of Mn_3O_4/r-GO, bare Mn_3O_4, r-GO and GO. The most intensive peak of GO is found at *ca*. 10.23°, corresponding to the (001) reflection with the interlayer spacing (0.9 nm), which also indicates that the rich oxygen-containing functional groups are introduced on the surface of GO. The sharp characteristic peaks are observed in the XRD patterns of the bare Mn_3O_4 and Mn_3O_4/r-GO, indicating the formation of highly crystallized phases. Their crystalline structure could be assigned to the hausmannite Mn_3O_4 (JCPDS 75-1560). The r-GO sample shows a broader peak in the 2θ range of 20-30°, however, no obvious diffraction peaks of the r-GO nanosheets are detected in the Mn_3O_4/r-GO composite, indicating

that the r-GO nanosheets are sufficiently separated by the Mn_3O_4 nanoparticles.

The microstructure of the Mn_3O_4/r-GO and bare Mn_3O_4 was investigated by SEM and TEM. As shown in Figure 3(a, b), the bare Mn_3O_4 particles show spherical-like morphology, but the particles are severely aggregated together, giving rise to a big particle size. By comparison, we can observe that the size of the Mn_3O_4 particles, prepared by a same procedure in the presence of GO, is dramatically decreased. This is because a strong interaction between Mn_3O_4 particles and r-GO sheets drastically limits the growth and the agglomeration of the crystalline Mn_3O_4 particles to some extent. The TEM image in Figure 3(c) indicates that Mn_3O_4 nanoparticles with a small size of 20-30 nm are uniformly dispersed on the surface of r-GO and no free particles are detected. The high-resolution TEM image in Figure 3(d) further reveals that the Mn_3O_4 particles are closely attached on r-GO nanosheets. The crystal lattice fringes with d-spacing of 0.25 nm can be assigned to the (202) crystal plane of tetragonal Mn_3O_4. Based on these observations, it can be concluded that such a combination of Mn_3O_4 particles with r-GO sheets can enable fast electron transport through the conductive matrix to Mn_3O_4 particles, guaranteeing efficient electrochemical performance.

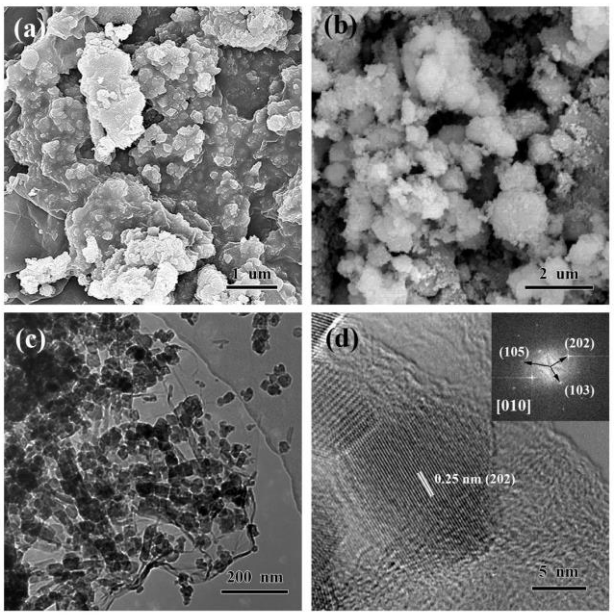

Figure 3 Typical SEM images of (a) Mn_3O_4/r-GO and (b) bare Mn_3O_4; (c) Low-magnification TEM image and (d) high-resolution TEM image obtained along [010] zone axis of Mn_3O_4/r-GO.

To study the lithium storage properties of the Mn_3O_4/r-GO composite, a series of electrochemical measurements were carried out. The specific capacity is based on the mass of Mn_3O_4 in the composite. Figure 4(a) shows the charge-discharge profiles of the Mn_3O_4/r-GO composite. The first discharge and charge capacities of the Mn_3O_4/r-GO composites are 1912 and 1296 mAh g^{-1}, respectively, accounting for an initial Coulombic efficiency of 67.8 %. The large capacity loss in the first cycle is mainly attributed to the irreversible processes such as the electrolyte decomposition, inevitable formation of solid electrolyte interphase (SEI) layer and the reaction of oxygenated functional groups unreduced on the surface of r-GO. In the subsequent cycles, the Mn_3O_4/r-GO electrode exhibits high reversibility and stability, evidenced from the almost overlapped charge or discharge curves. The discharge and charge capacities at the 10th cycle are 1198 and 1141 mAh g^{-1}, respectively. The

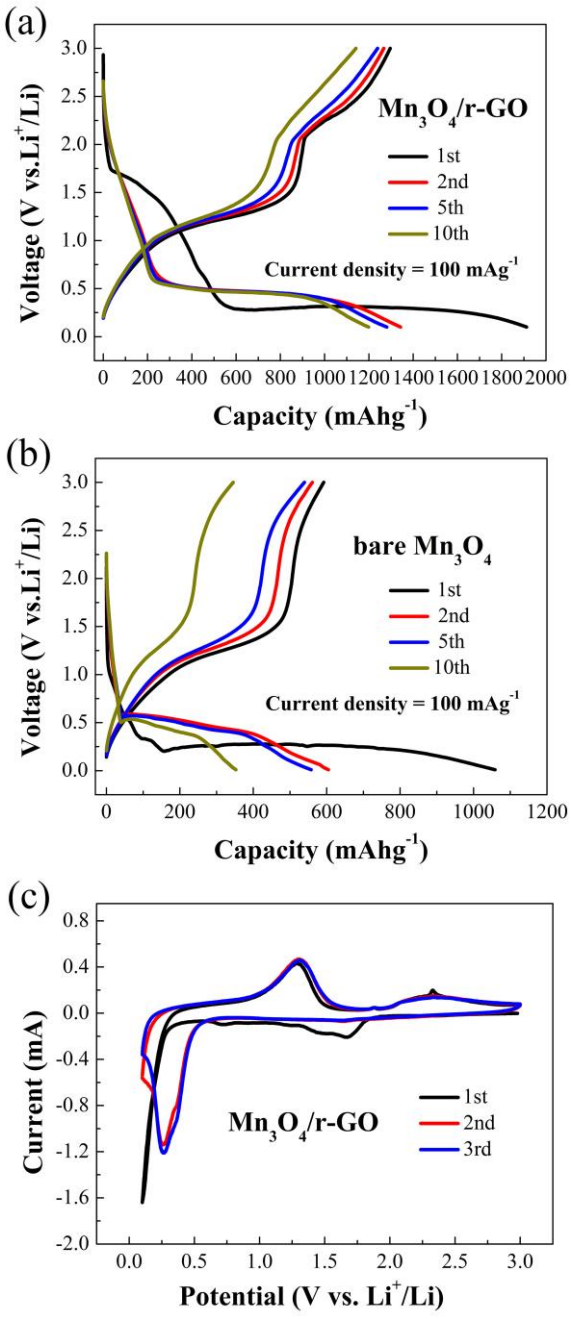

Figure 4 Galvanostatic charge-discharge profiles of (a) Mn_3O_4/r-GO composite and (b) bare Mn_3O_4 at the 1st, 2nd, 5th and 10th cycle; (c) CV plots of Mn_3O_4/r-GO composite at 0.1 mV s^{-1}.

columbic efficiency is remarkably increased to 95.2%. Very interestingly, the Mn_3O_4/r-GO composite shows a high specific

capacity than the theoretical value of bulk Mn_3O_4 (937 mAh g^{-1}). This is a normal phenomenon in metal oxide anode materials for lithium storage. Most of this extra capacity could be due to additional lithium storage in the grain boundaries of Li_2O and metal formed in the reduction cycle. Recently, Grey *et al.*[33] have investigated the origin of extra capacity in metal oxide electrodes. Their experiments and theoretical calculations revealed that a major contribution to the extra capacity is due to the generation of LiOH and its subsequent reversible reaction with Li to form Li_2O and LiH. Figure 4(b) presents discharge-charge profiles of the bare Mn_3O_4 particles. In contrast, the low specific capacity and rapid capacity fade are observed for bare Mn_3O_4. Figure 4(c) show the CV plots of Mn_3O_4/r-GO composite. After the first cycle, the profiles of CV curves become almost overlapped. A stable cathodic peak at 0.3 V, and two anodic peaks at around 1.3, 2.4 V are observed in the CV scan, indicating the good reversible cycling of the Mn_3O_4/r-GO composite electrode.

Furthermore, in order to illustrate the role of the microexplosion reaction originated from the decomposition of H_2O_2, the Mn_3O_4/r-GO composite was also synthesized without adding H_2O_2 during the preparation process and its SEM image is shown in Figure S1 (Supporting Information). It is clear that the resulting Mn_3O_4/r-GO composite is less uniform than the composite synthesized by adding H_2O_2 (Figure 1a). Figure S2 shows the Nitrogen adsorption-desorption isotherms of two Mn_3O_4/r-GO composites synthesized with and without adding H_2O_2. It can be calculated that the BET specific surface area of the Mn_3O_4/r-GO composite without adding H_2O_2 is 12.98 m^2 g^{-1}, which is much smaller than that of the composite with adding H_2O_2 (81.07 m^2 g^{-1}). Figure S3 demonstrates the charge-discharge profiles of the composite synthesized without adding H_2O_2. In comparison with that shown in Figure 4a, the first discharge and charge capacities of the Mn_3O_4/r-GO composite synthesized without microexplosion reaction are much lower (1259 and 889 mAh g^{-1}, respectively). In the subsequent cycles, this composite shows a low specific capacity and poor stability with respect to the Mn_3O_4/r-GO composite synthesized through microexplosion reaction process. These results reveal that the microexplosion synthesis process really exfoliates the r-GO flakes and improve electrochemical properties of the composite material.

Figure 5(a) shows the rate capability of the Mn_3O_4/r-GO composite at a current density ranging from 0.2 to 2 A g^{-1} for 10 cycles at each rate. It can be found that the discharge and charge capacities remain stable and decrease regularly with an increased rate. The final reversible capacities of the composite are measured as 870, 660, 450, 310 and 180 mAh g^{-1} at the current densities of 0.2, 0.4, 0.8, 1 and 2 A g^{-1}, respectively. It is also noted that the charge and discharge capacities at various rates are nearly the same, indicative of high reversibility. When the current density returns to 0.2A g^{-1}, the specific capacity can be recovered (even a little higher than the original capacity). The results reveal that the Mn_3O_4/r-GO composite has good rate capability and cycling stability. In order to further highlight the superiority of the Mn_3O_4/r-GO composite as anode material for LIBs, the cycling performance of the Mn_3O_4/r-GO composite and bare Mn_3O_4 at 1.2 A g^{-1} is compared in Figure 5(b). In the initial 100 cycles, the capacity of the Mn_3O_4/r-GO composite exhibits a rapid fade from 370 to 210 mAh g^{-1}, and then gradually increases to 330 mAh g^{-1} at the 250th cycle and keeps relatively stable during the further cycling. This phenomenon is well-documented in the literature related to the metal oxide electrode materials and is attributed to the reversible growth of a polymeric gel-like film resulting from kinetically activated electrolyte degradation.[16, 34-36] Compared with the Mn_3O_4/r-GO composites, the bare Mn_3O_4 delivers a low specific capacity below than 50 mAh g^{-1} throughout the whole cycling process. Such inferior properties can be ascribe to its poor electrical conductivity.

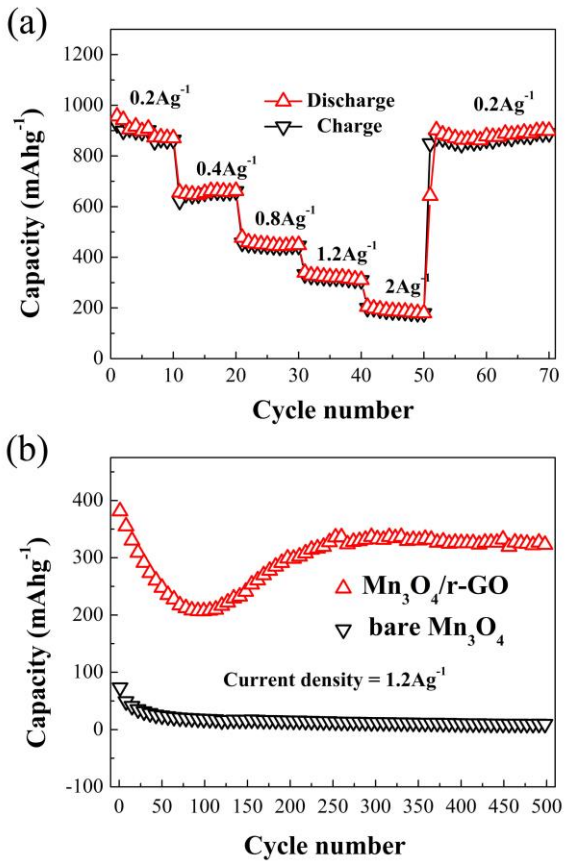

Figure 5 (a) Rate capability of Mn_3O_4/r-GO composite; (b) Cycle performance of Mn_3O_4/r-GO composite and bare Mn_3O_4 at 1.2 A g^{-1}.

From the comparison between the Mn_3O_4/r-GO composite and bare Mn_3O_4, we conclude that the excellent electrochemical performance, including high reversible capacity, improved cycle stability, and high rate performance of the composite, can be ascribed to the following factors: Firstly, the r-GO sheets play a role as an excellent mini-current collector, which effectively enhance the electrical conductivity of Mn_3O_4 for the rapid electrochemical reactions. Secondly, the r-GO sheets may act as a flexible two-dimensional support for homogeneous anchoring of Mn_3O_4 nanoparticles, which not only provides an elastic buffer space to accommodate large volume changes induced by lithium insertion/extraction, but also confines the growth and aggregation of Mn_3O_4 upon continuous cycling.

4. Conclusion

In summary, we have developed a novel microexplosion method to synthesize the Mn_3O_4/r-GO composite. The ultrafine Mn_3O_4 nanoparticles with the average size of about 20 nm are uniformly dispersed on the r-GO sheets. In comparison with the bare Mn_3O_4, the Mn_3O_4/r-GO composite exhibits better electrochemical properties, including a high reversible specific capacity of more than 1100 mAh g^{-1} at 0.1 A g^{-1}. Even at a high current density of 1.2 A g^{-1}, this material still can achieve an acceptable capacity of 330 mAh g^{-1}. In addition, the most attractive property of this composite should be its extraordinary rate capability related to the bare Mn_3O_4. Our results clearly demonstrate that this kind of Mn_3O_4/r-GO composite is a good candidate for high-performance LIBs anode materials.

Acknowledgements

This work was supported by the National Natural Science Foundation of China (20673100, 51201151, 51172205, 51002138), the Natural Science Foundation of Zhejiang Province (LY13E020010, LR13E020002), Scientific Research Fund of Zhejiang Provincial Education Department (Y201432424) and New Century Excellent Talents in University (NCET 111079).

References

1. P. Poizot, S. Laruelle, S. Grugeon, L. Dupont and J. Tarascon, *Nature*, 2000, **407**, 496-499.
2. Y. P. Gan, H. Q. Gu, H. Xiao, Y. Xia, X. Y. Tao, H. Huang, J. Du, L. S. Xu and W. K. Zhang, *New J. Chem.*, 2014, DOI: 10.1039/c4nj00090k.
3. N. D. Petkovich, S. G. Rudisill, B. E. Wilson, A. Mukherjee and A. Stein, *Inorg. chem.*, 2014, **53**,1100-1112.
4. W.-Y. Li, L.-N. Xu and J. Chen, *Adv. Funct. Mater.s*, 2005, **15**, 851-857.
5. Z.-S. Wu, W. Ren, L. Wen, L. Gao, J. Zhao, Z. Chen, G. Zhou, F. Li and H.-M. Cheng, *ACS nano*, 2010, **4**, 3187-3194.
6. H. Huang, W. Zhu, X. Tao, Y. Xia, Z. Yu, J. Fang, Y. Gan and W. Zhang, *ACS Appl. Mater. Inter.*, 2012, **4**, 5974-5980.
7. P.-L. Taberna, S. Mitra, P. Poizot, P. Simon and J.-M. Tarascon, *Nat. Mater.*, 2006, **5**, 567-573.
8. Y. S. Kang, S. Risbud, J. F. Rabolt and P. Stroeve, *Chem. Mater.*, 1996, **8**, 2209-2211.
9. H. Xiao, Y. Xia, W. K. Zhang, H. Huang, Y. P. Gan and X. Y. Tao, *J. Mater. Chem. A*, 2013, **1**, 2307-2312.
10. Z. Xiao, Y. Xia, Z. H. Ren, Z. Y. Liu, G. Xu, C. Y. Chao, X. Li, G. Shen and G. R. Han, *J. Mater. Chem.*, 2012, **22**, 20566-20573.
11. H. Guan, X. Wang, H. Li, C. Zhi, T. Zhai, Y. Bando and D. Golberg, *Chem. Commun.*, 2012, **48**, 4878-4880.
12. N. Yan, L. Hu, Y. Li, Y. Wang, H. Zhong, X. Hu, X. Kong and Q. Chen, *J. Phys. Chem. C*, 2012, **116**, 7227-7235.
13. B. Guo, C. Li and Z.-Y. Yuan, *J. Phys. Chem. C*, 2010, **114**, 12805-12817.
14. H. Kim, S.-W. Kim, J. Hong, Y.-U. Park and K. Kang, *J. Mater. Res.*, 2011, **26**, 2665-2671.
15. Y. Xia, Z. Xiao, X. Dou, H. Huang, X. H. Lu, R. J. Yan, Y. P. Gan, W. J. Zhu, J. P. Tu, W. K. Zhang and X. Y. Tao, *ACS nano*, 2013, **7**, 7083-7092.
16. C. Wang, L. Yin, D. Xiang and Y. Qi, *ACS Appl. Mater. Inter.*, 2012, **4**, 1636-1642.
17. I. Nam, N. D. Kim, G.-P. Kim, J. Park and J. Yi, *J. Power Sources*, 2013, **244**, 56-62.
18. H. Wang, L.-F. Cui, Y. Yang, H. Sanchez Casalongue, J. T. Robinson, Y. Liang, Y. Cui and H. Dai, *J. Am. Chem. Soc.*, 2010, **132**, 13978-13980.
19. L. Li, Z. Guo, A. Du and H. Liu, *J. Mater. Chem.*, 2012, **22**, 3600-3605.
20. L.-F. Cui, Y. Yang, C.-M. Hsu and Y. Cui, *Nano Lett.*, 2009, **9**, 3370-3374.
21. K. Wang, X. He, L. Wang, J. Ren, C. Jiang and C. Wan, *Solid State Ionics*, 2007, **178**, 115-118.
22. Z.-H. Wang, L.-X. Yuan, Q.-G. Shao, F. Huang and Y.-H. Huang, *Mater. Lett.*, 2012, **80**, 110-113.
23. S. Zhang, Y. Li, G. Xu, S. Li, Y. Lu, O. Toprakci and X. Zhang, *J. Power Sources*, 2012, **213**, 10-15.
24. C. Chen, H. Jian, X. Fu, Z. Ren, M. Yan, G. Qian and Z. Wang, *RSC Adv.*, 2014, **4**, 5367-5370.
25. J. Duan, Y. Zheng, S. Chen, Y. Tang, M. Jaroniec and S. Qiao, *Chem. Commun.*, 2013, **49**, 7705-7707.
26. J. Gao, M. A. Lowe and H. D. Abruna, *Chem. Mater.*, 2011, **23**, 3223-3227.
27. A. Yu, H. W. Park, A. Davies, D. C. Higgins, Z. Chen and X. Xiao, *J. Phys. Chem. Lett.*, 2011, **2**, 1855-1860.
28. F. Zeng, Y. Kuang, Y. Wang, Z. Huang, C. Fu and H. Zhou, *Adv. Mater.*, 2011, **23**, 4929-4932.
29. N. Li, Z. Geng, M. Cao, L. Ren, X. Zhao, B. Liu, Y. Tian and C. Hu, *Carbon*, 2013, **54**, 124-132.
30. Q. Jiangying, G. Feng, Z. Quan, W. Zhiyu, H. Han, L. Beibei, W. Wubo, W. Xuzhen and Q. Jieshan, *Nanoscale*, 2013, **5**, 2999-3005.
31. W. S. Hummers Jr and R. E. Offeman, *J. Am. Chem. Soc.*, 1958, **80**, 1339-1339.
32. L. Fu, H.-b. LIU, Y.-h. ZOU and B. LI, *Carbon*, 2005, **4**, 10-14.
33. Y.-Y. Hu, Z. Liu, K.-W. Nam, O. J. Borkiewicz, J. Cheng, X. Hua, M. T. Dunstan, X. Yu, K. M. Wiaderek and L.-S. Du, *Nat. mater.*, 2013,**12**, 1130–1136
34. Y.-M. Lin, P. R. Abel, A. Heller and C. B. Mullins, *J. Phys. Chem. Lett.*, 2011, **2**, 2885-2891.
35. R. Wang, C. Xu, J. Sun, Y. Liu, L. Gao and C. Lin, *Nanoscale*, 2013, **5**, 6960-6967.
36. X. Rui, H. Tan, D. Sim, W. Liu, C. Xu, H. H. Hng, R. Yazami, T. M. Lim and Q. Yan, *J. Power Sources*, 2013, **222**, 97-102.